

Article

State-of-Charge Estimation of Lithium-Ion Batteries Based on Dual-Coefficient Tracking Improved Square-Root Unscented Kalman Filter

Simin Peng ¹, Ao Zhang ¹ , Dandan Liu ¹, Mengzeng Cheng ², Jiarong Kan ¹ and Michael Pecht ^{3,*} 

¹ School of Electrical Engineering, Yancheng Institute of Technology, Yancheng 224051, China; siminpeng@ycit.edu.cn (S.P.)

² Economic Research Institute of State Grid Liaoning Electric Power Supply Co., Ltd., Shenyang 110015, China

³ Center for Advanced Life Cycle Engineering (CALCE), University of Maryland, College Park, MD 20742, USA

* Correspondence: pecht@umd.edu

Abstract: Accurate state of charge (SOC) estimation is helpful for battery management systems to extend batteries' lifespan and ensure the safety of batteries. However, due to the pseudo-positive definiteness of the covariance matrix and noise statistics error accumulation, the SOC estimation of lithium-ion batteries is usually inaccurate or even divergent using Kalman filters, such as the unscented Kalman filter (UKF) and the square-root unscented Kalman filter (SRUKF). To resolve this problem, an SOC estimation method based on the dual-coefficient tracking improved square-root unscented Kalman filter for lithium-ion batteries is developed. The method is composed of an improved square-root unscented Kalman filter (ISRUkf) and a dual-coefficient tracker. To avoid the divergence of SOC estimation due to the covariance matrix with pseudo-positive definiteness, an ISRUkf based on the QR decomposition covariance square-root matrix is presented. Moreover, the dual-coefficient tracker is designed to track and correct the state noise error of the battery, which can reduce the SOC estimation error caused by the accumulation of the battery model error using the ISRUkf. The accuracy and robustness of the SOC estimation method using the developed method are validated by the comparison with the UKF and SRUKF. The developed algorithm shows the highest SOC estimation accuracy with the SOC error within 1.5%.



Citation: Peng, S.; Zhang, A.; Liu, D.; Cheng, M.; Kan, J.; Pecht, M. State-of-Charge Estimation of Lithium-Ion Batteries Based on Dual-Coefficient Tracking Improved Square-Root Unscented Kalman Filter. *Batteries* **2023**, *9*, 392. <https://doi.org/10.3390/batteries9080392>

Academic Editor: Carlos Zieber

Received: 6 June 2023

Revised: 9 July 2023

Accepted: 24 July 2023

Published: 26 July 2023



Copyright: © 2023 by the authors. Licensee MDPI, Basel, Switzerland. This article is an open access article distributed under the terms and conditions of the Creative Commons Attribution (CC BY) license (<https://creativecommons.org/licenses/by/4.0/>).

1. Introduction

Lithium-ion batteries have been widely used in electric vehicles and battery energy storage [1,2] due to the advantages of a high energy density, long cycle life, and low self-discharge rate [3–5]. The battery management system is indispensable to the monitoring and estimation of the critical internal states of lithium-ion batteries [6]. Furthermore, state of charge (SOC) estimation is one of the battery management system's most important state parameters [7–9]. Accurate SOC estimation helps the battery management system to optimize the operation characteristics, eliminating potential safety risks and prolonging the batteries' lifespan [10]. However, it is difficult to accurately estimate the SOC in complex driving environments due to the nonlinear electrochemical performance of lithium-ion batteries and the SOC immeasurability [11].

Recently, other literature has been published to accurately estimate the SOC for lithium-ion batteries. In general, the SOC estimation method can be classified into four groups: the looking-up table-based method, ampere-time integration method, data-driven method, and model-based method [12]. In the looking-up table-based method, the initial SOC value is determined by the open-circuit voltage (OCV) collected using the battery management system, and the SOC value is attained by the SOC-OCV correspondence table via the subsequent OCV measurement value [13]. However, it is more suitable for application in a

laboratory environment because of its drawbacks, such as being time-consuming and susceptible to external environment influences in batteries' temperature and aging conditions. The ampere-time integration method estimates the SOC by integrating the currents flowing into and out of the batteries over time. The SOC estimation based on this method depends on SOC initial errors and current measurement errors, which results in increasing SOC estimation errors [14–16]. Data-driven methods—such as the neural network method [17], support vector machine method [18], and Bayesian network method [19,20]—are studied to accurately estimate the SOC for a nonlinear system.

These methods are not suitable for practical SOC estimation online, though, due to the requirements of an enormous amount of training data and the high calculation cost. Model-based methods consisting of the batteries' equivalent circuit model (ECM) and a filter—such as a Kalman filter (KF) and particle filter (PF)—are attracting extensive attention and becoming one of the most popular algorithms to accurately estimate the SOC for lithium-ion batteries [21].

Compared with the PF, which requires many particles to calculate the posterior probability density, the KF can reduce the number of sampled particles and ensure the accuracy requirements with the help of deterministic sampling. The standard KF is a widely used linear filter but has poor adaptability to nonlinear time-varying systems [22]. As an improved method of the KF, the extended Kalman filter (EKF) can be used in nonlinear time-varying systems. However, the SOC estimation accuracy using the EKF is degraded due to its requirements of the Jacobian matrix calculation and a linearized approximation of the nonlinear time-varying function using the first-order terms of the Taylor formula, which does not consider the higher-order terms of the Taylor formula [23].

To resolve the disadvantages of the KF and the EKF noted above, the unscented Kalman filter (UKF) is presented to estimate the SOC [24]. The UKF based on unscented transform does not need to linearize system equations without accounting for the higher-order terms of the Taylor formula, and the UKF shows higher SOC estimation accuracy than the EKF. SOC estimation using the UKF will be divergent because of its drawbacks, such as the pseudo-positive definiteness of the covariance matrix caused by the error accumulation in the UKF. To resolve these shortcomings, the square-root unscented Kalman filter (SRUKF) is presented to estimate the batteries' SOC [25–29]. Compared to the UKF, the SRUKF uses the state covariance square-root matrix instead of the state covariance matrix, which can overcome the problem of the pseudo-positive definiteness of the covariance matrix. The SOC estimation accuracy based on the SRUKF will be reduced because the SRUKF needs to use the Cholesky decomposition method to achieve the state covariance square-root matrix.

Moreover, the SOC estimation accuracy based on the KF mentioned above is greatly degraded by unknown or inaccurate noise statistics, such as the measurement and model noise covariance of the batteries [30]. In the iteration process of these KFs, the calculation accuracy of the system covariance matrix is dependent on the accurate noise statistics. The error accumulation of noise statistics will be generated in the iteration process, which leads to the divergence of the KFs. An adaptive EKF based on the combination of adaptive modification and the EKF is proposed to avoid the divergence of the algorithm error [31]. Based on the UKF and an adaptive noise estimator established by noise covariance matching, an adaptive unscented Kalman filter (AUKF) is developed to estimate the SOC. The SOC estimation accuracy using the AUKF is improved for the battery system with uncertain noise statistics [32], but its accuracy is still degraded because of not considering the state noise error accumulative calculation in the iteration process of the AUKF.

As mentioned above, the discharging and charging process of lithium-ion batteries is a nonlinear electrochemical reaction process. It is difficult to accurately attain the SOC of lithium-ion batteries due to their nonlinear operating characteristics. Model-based methods consisting of the KF and its improved algorithms, such as the UKF, the AUKF, and the SRUKF, are widely used to estimate the SOC of the batteries. However, the estimated SOC using these KFs will be divergent due to their drawbacks, such as the pseudo-positive definiteness of the covariance matrix in the UKF and the Cholesky decomposition in the

SRUKF. Moreover, the SOC estimation accuracy is degraded by the inaccurate model noise covariance and its accumulative error of the batteries using these model-based methods, including the UKF, the SRUKF, and the AUKF. To solve these problems, a dual-coefficient tracking ISRUKEF is developed to achieve accurate SOC estimation for lithium-ion batteries with uncertain noise statistics. The innovation of the developed method includes the following: (1) To avoid the divergence of SOC estimation due to the pseudo-positive definiteness of the state covariance matrix, the ISRUKEF based on the QR decomposition method of the state covariance square-root matrix is presented. (2) A dual-coefficient tracker based on the strong tracking filter (STF) is designed to track and correct the state noise error accumulation of the battery, which can reduce the SOC estimation error caused by the batteries' model error accumulation using the UKF and the ISRUKEF. (3) An SOC estimation method based on the ISRUKEF and the dual-coefficient tracker is developed for lithium-ion batteries with uncertain noise statistics.

The rest of this paper is organized as follows: Section 2 introduces the construction of the ECM and its state space equation of lithium-ion batteries; Section 3 presents the developed SOC estimation method based on dual-coefficient tracking ISRUKEF, including the ISRUKEF and the dual-coefficient tracker; Section 4 shows the accuracy and robustness of the developed SOC estimation method by the comparison of the simulation results and the experimental data in different conditions; and Section 5 discusses the conclusions.

2. Equivalent Circuit Model and State Space Equation of Lithium-Ion Batteries

2.1. Equivalent Circuit Model of the Batteries

Since it can accurately describe the dynamic characteristics of the batteries [33], an ECM based on a two-order RC circuit in this paper is shown in Figure 1. U_{OC} describes the open circuit voltage of the batteries; R_0 represents the batteries' internal resistance; R_L illustrates the concentration resistance; C_L is the concentration capacitance; R_S represents the electrochemical resistance; C_S means the electrochemical capacitance; I_t is the current of the batteries; and U_t is the terminal voltage of the batteries that is connected to the loads.

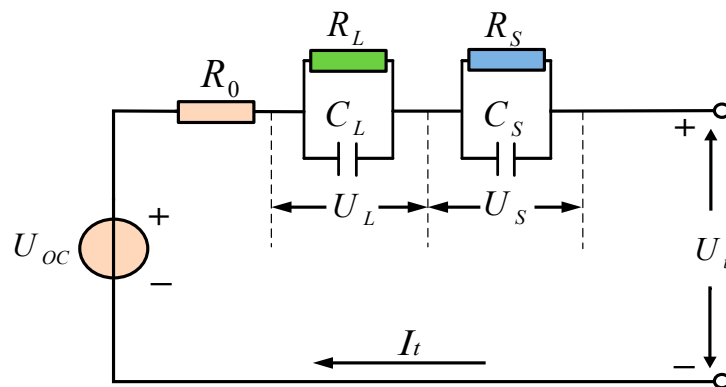


Figure 1. Equivalent circuit model of the batteries.

As shown in Figure 1, according to Kirchhoff's voltage law, the functional relationship between the terminal voltage U_t and the current of the batteries I_t can be expressed as:

$$U_t = U_{OC} - U_S - U_L - I_t R_0 \quad (1)$$

where U_S represents the electrochemical voltage of the batteries, and U_L means the concentration voltage of the batteries.

In the ECM of the batteries, according to the experimental data of the batteries in the charging and discharging process, the nonlinear functional relationship between R_0 , R_L , C_L , R_S , C_S , and the SOC can be achieved by the least-squares-error curve-fitting method, which can be represented as:

$$U_{OC}(t) = a_0 e^{-a_1 SOC(t)} + a_2 + a_3 SOC(t) - a_4 SOC^2(t) + a_5 SOC^3(t) \quad (2)$$

$$R_0(t) = b_0 e^{-b_1 SOC(t)} + b_2 + b_3 SOC(t) - b_4 SOC^2(t) + b_5 SOC^3(t) \quad (3)$$

$$R_L(t) = c_0 e^{-c_1 SOC(t)} + c_2 \quad (4)$$

$$C_L(t) = d_0 e^{-d_1 SOC(t)} + d_2 \quad (5)$$

$$R_S(t) = e_0 e^{-e_1 SOC(t)} + e_2 \quad (6)$$

$$C_S(t) = f_0 e + f_1 SOC(t) + f_2 \quad (7)$$

where $a_0 \sim a_5$, $b_0 \sim b_5$, $c_0 \sim c_2$, $d_0 \sim d_2$, $d_0 \sim d_2$, and $f_0 \sim f_2$ are the coefficients, which can be obtained by the least-squares-error curve-fitting method via the experimental data.

The SOC, which represents the percentage of the current battery capacity in the total battery capacity, can be expressed as:

$$SOC(t) = SOC_0 - \frac{\int \eta I_t dt}{Q_N} \quad (8)$$

where SOC_0 means the initial value of SOC, η shows coulomb efficiency, and Q_N denotes the nominal capacity.

2.2. State Space Equation of the Battery Model

To describe the battery model in state space equations, the SOC, the electrochemical voltage U_S and the concentration voltage U_L are selected as battery state variables. The I_t is chosen as the input variables of the batteries, and the U_t is assumed to be the output variables of the batteries. According to the SOC expression in (8) and the batteries' ECM as shown in Figure 1, the state space equation of the batteries in discrete time can be written as:

$$\begin{bmatrix} SOC_{k+1} \\ U_{S,k+1} \\ U_{L,k+1} \end{bmatrix} = \begin{bmatrix} 1 & 0 & 0 \\ 0 & e^{(-\Delta t/\tau_1)} & 0 \\ 0 & 0 & e^{(-\Delta t/\tau_2)} \end{bmatrix} \begin{bmatrix} SOC_k \\ U_{S,k} \\ U_{L,k} \end{bmatrix} + \begin{bmatrix} -\eta \Delta t / Q_N \\ R_S \left[1 - e^{(-\Delta t/\tau_1)} \right] \\ R_L \left[1 - e^{(-\Delta t/\tau_2)} \right] \end{bmatrix} I_{t,k} + w_k \quad (9)$$

where Δt represents the sampling time; $\tau_1 \sim \tau_2$ illustrates the time constant, $\tau_1 = R_S C_S$, and $\tau_2 = R_L C_L$; and w_k is the state noise.

Moreover, the measurement equation of the batteries in discrete time can be expressed as:

$$U_{t,k+1} = U_{OC,k+1} - U_{S,k+1} - U_{L,k+1} - I_{t,k+1} R_{0,k+1} + v_{k+1} \quad (10)$$

where v_k is the measurement noise.

3. SOC Estimation Based on the Dual-Coefficient Tracking ISRUKF

Due to not considering the higher-order terms of the Taylor formula, the SOC estimation based on the EKF is inaccurate. Compared to using the EKF, the SOC estimation accuracy is higher using the UKF since it does not require the Jacobian matrix calculation. However, the UKF's SOC estimation accuracy and stability are degraded given the pseudo-positive definiteness of the covariance matrix and the inaccurate noise statistics. The SRUKF based on the Cholesky decomposition method can partly reduce the influence of the pseudo-positive definiteness of the covariance matrix in the iteration process, but the SRUKF does not completely resolve the problem of pseudo-positive definiteness due to its nonlinear state calculation.

In this paper, a dual-coefficient tracking ISRUKF is developed to improve SOC estimation accuracy in two ways. First, the ISRUKF based on the QR decomposition method

can overcome the problem of the pseudo-positive definiteness of the covariance matrix in the UKF and the SRUKF. Second, a dual-coefficient tracker based on the STF is designed to track and correct the batteries' state noise error. In the dual-coefficient tracker, the tracking coefficient of state noise δ_k is used to adaptively track and correct the state noise error, and the fading factor λ_k of the STF is used to track and adjust the state covariance square-root matrix. The diagram of the developed ISRUKF is shown in Figure 2.

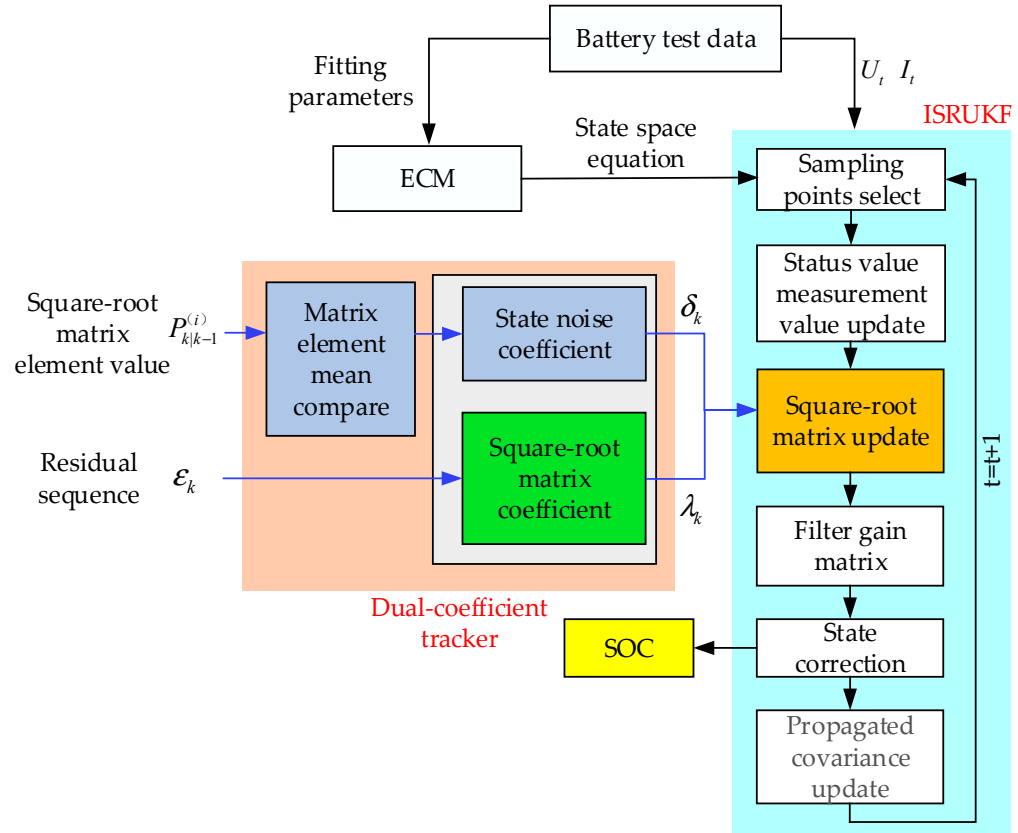


Figure 2. Diagram of the developed ISRUKF.

3.1. Improved Square-Root Unscented Kalman Filter (ISRUKF)

3.1.1. Standard SRUKF

For a nonlinear discrete time system, the system state equation and the system measurement equation can be described as:

$$\begin{cases} x_k = f(x_{k-1}, u_k) + w_k \\ y_k = g(x_k, u_k) + v_k \end{cases} \quad (11)$$

where x_k is the system state vector; y_k is the system measurement vector; $f(\cdot)$ and $g(\cdot)$ denote the nonlinear state and measurement models, respectively; u_k is the system input vector; w_k and v_k are the system state noise and measurement noise, respectively, and their statistics characteristics can be expressed as:

$$\begin{cases} E[w_k] = q, cov(w_k, w_j) = Q \\ E[v_k] = r, cov(v_k, v_j) = R \\ cov(w_k, v_j) = 0 \end{cases} \quad (12)$$

where r and q denote the mean value of v_k and w_k separately. R and Q denote the covariance value of v_k and w_k , respectively. The detailed steps of the SRUKF can be summarized as follows:

- (1) Initialize the mean (x_0) and the state covariance square root (S_0) of the system state:

$$\begin{cases} \hat{x}_0 = E(x_0) \\ S_0 = \sqrt{E[(x_0 - \hat{x}_0)(x_0 - \hat{x}_0)^T]} \end{cases} \quad (13)$$

where $E(\cdot)$ is the expectation mean value, and $(\cdot)^T$ is the matrix transpose operation.

(2) Assign weights and obtain sampling points:

$$\begin{cases} x_{0,k} = \hat{x}_k \\ x_{i,k} = \hat{x}_k + \sqrt{(n + \lambda)S_{k|k}} \\ x_{i+n,k} = \hat{x}_k - \sqrt{(n + \lambda)S_{k|k}} \end{cases} \quad (14)$$

where n represents the dimension of the state vector, and λ means a scale that can be presented as:

$$\lambda = \alpha^2(n + h) - n \quad (15)$$

where α is a scaling parameter, its range is set as 0~1, h is the column factor, and $h = 3 - n$.

The weighted coefficients can be expressed as

$$\begin{cases} w_0^m = \frac{\lambda}{n+\lambda} \\ w_0^c = \frac{\lambda}{n+\lambda} + (1 + \beta - \alpha^2) \\ w_i^m = w_i^c = \frac{1}{2(n+\lambda)} \end{cases} \quad (16)$$

where w^m is the variance weight factor; w^c is the mean weight factor; and β is the error magnitude of the higher-order term.

(3) Time update for the system states:

a. Update the sample point:

$$x_{i,k|k-1} = f(x_{i,k-1}) \quad (17)$$

b. Estimate the system state:

$$\hat{x}_{k|k-1} = \sum_{i=0}^{2n} w_i^m x_{i,k|k-1} + q_k \quad (18)$$

c. Update the covariance of the estimated state:

$$S_{k|k-1}^* = qr \left\{ \left[\sqrt{w_i^c} (x_{i=1:2n,k|k-1} - \hat{x}_{k|k-1}), \sqrt{Q_{k-1}} \right] \right\}, i = 1, 2, \dots, 2n \quad (19)$$

$$S_{k|k-1} = cholupdate\{S_{k|k-1}^*, x_{i,k|k-1} - \hat{x}_{k|k-1}, w_0^c\} \quad (20)$$

where $S_{k|k-1}^*$ is the updated state calculation value; $qr(\cdot)$ is the QR decomposition; $S_{k|k-1}$ is the state covariance square-root matrix; and $cholupdate(\cdot)$ is the Cholesky decomposition.

(4) Measurement update:

a. Attain the measurement:

$$y_{i,k|k-1} = g(x_{i,k|k-1}) \quad (21)$$

b. Update the measurement:

$$\hat{y}_{k|k-1} = \sum_{i=0}^{2n} w_i^m y_{i,k|k-1} + r_k \quad (22)$$

(5) Calculate the SRUKF gain matrix L :

$$L_k = P_{xy} / S_z S_z^T \quad (23)$$

where P_{xy} is the mutual covariance, as shown in Formula (24), and S_z is the measurement covariance square-root matrix, as shown in Formula (26).

$$P_{xy} = \sum_{i=0}^{2n} w_i^c (x_{i,k|k-1} - \hat{x}_{k|k-1}) (y_{i,k|k-1} - \hat{y}_{k|k-1})^T \quad (24)$$

$$S_z^* = qr\{[\sqrt{w_i^c}(\hat{y}_{i=1:2n,k|k-1} - \hat{y}_{k|k-1}), \sqrt{R_{k-1}}]\} \quad (25)$$

$$S_z = cholupdate\{S_z^*, y_{i,k|k-1} - \hat{y}_{k|k-1}, w_0^c\} \quad (26)$$

where S_z^* is the updated calculation measurement.

(6) Measurement correction:

a. Update the estimated state:

$$\hat{x}_{k|k} = \hat{x}_{k|k-1} + L_k (y_k - \hat{y}_{k|k-1}) \quad (27)$$

b. Update the propagated covariance:

$$S_{k|k} = cholupdate\{S_{k|k-1}, L_k S_z, -1\} \quad (28)$$

where $S_{k|k}$ is the state covariance square-root optimal estimation matrix.

3.1.2. The ISRUKF Based on the QR Decomposition Method

As seen from Formula (20) in the standard SRUKF, the SRUKF requires the Cholesky decomposition to obtain the state covariance square-root matrix $S_{k|k-1}$. Due to the matrix computation errors in the Cholesky decomposition, the SRUKF estimation accuracy will be degraded by the pseudo-positive definiteness of the $S_{k|k-1}$. To solve this problem, the ISRUKF based on the QR decomposition method is developed in this paper. The detailed core concept of the ISRUKF based on the QR decomposition method is presented as follows.

The formula of the state covariance matrix $P_{k|k-1}$ can be described as

$$P_{k|k-1} = \sum_{i=0}^{2n} w_i^c [x_{i,k|k-1} - \hat{x}_{k|k-1}] [\hat{x}_{k|k-1} - \hat{x}_{k|k-1}]^T + Q_{k-1} \quad (29)$$

Then, the formula of the state covariance matrix $P_{k|k-1}$ and the state covariance square-root matrix $S_{k|k-1}$ is presented as

$$P_{k|k-1} = S_{k|k-1} S_{k|k-1}^T = [\sqrt{w_i^c}(x_{i,k|k-1} - \hat{x}_{k|k-1}), \sqrt{Q_{k-1}}][\sqrt{w_i^c}(x_{i,k|k-1} - \hat{x}_{k|k-1}), \sqrt{Q_{k-1}}]^T \quad (30)$$

we set $S_{k|k-1} = (q_k r_k)^T$; then

$$P_{k|k-1} = (q_k r_k)^T (q_k r_k) = r_k^T q_k^T q_k r_k = r_k^T r_k \quad (31)$$

where q_k is the upper triangular matrix, and r_k is the orthogonal matrix.

By combining Formulas (30) and (31), the following formula can be obtained

$$\begin{cases} r_k = qr\{[\sqrt{w_i^c}(x_{i=1:2n,k|k-1} - \hat{x}_{k|k-1}), \sqrt{Q_{k-1}}]^T\} \\ S_{k|k-1} = r_k^T \end{cases} \quad (32)$$

Substitute Formula (32) with Formula (20), which can effectively avoid the pseudo-positive qualitative problem existing in the standard SRUKF.

Similarly, Formulas (26) and (28) can be replaced by

$$\begin{cases} r_z = qr\{[\sqrt{w_i^c}(y_{i=1:2n,k|k-1} - \hat{y}_{k|k-1}), \sqrt{R_{k-1}}]^T\} \\ S_Z = r_k^T \end{cases} \quad (33)$$

$$\begin{cases} r_{k|k} = qr\{[(e - L_k H_k)S_{k|k-1}, L_k \sqrt{R_{k-1}}]^T\} \\ S_{k|k} = r_{k|k}^T \end{cases} \quad (34)$$

where e is the identity matrix of order n , and H_k is the coefficient matrix of the measurement function, which can be expressed as

$$H_k = (P_{xy})^T (S_{k|k-1} S_{k|k-1}^T) \quad (35)$$

3.2. The Dual-Coefficient Tracker Based on the Strong Tracking Filter

3.2.1. Strong Tracking Filter

The STF is used to attain the fading factor to update the state covariance square-root matrix in the iterative of the ISRUKF. The fading factor can be attained as

$$\begin{cases} S_{k|k-1} = \lambda_k S_{k|k-1} \lambda_k^T + \sqrt{Q_{k-1}} \\ \lambda_k = \text{diag}(\mu_0, \mu_k) \end{cases} \quad (36)$$

where λ_k is the fading factor, which is also the tracking coefficient of the state covariance square-root matrix, $\lambda_k = \text{diag}(\mu_0, \mu_k)$, $\mu_0 = [1, 1, \dots, 1]$, whose dimension is n columns, and $\mu_k = [u_k, u_k, u_k, \dots, u_k]$, which is described as

$$u_k = \begin{cases} \frac{\text{trace}(C_k - H_k Q_{k-1} H_k^T - R_{k-1})}{\text{trace}(P_{k|k-1} - Q_{k-1}) H_k^T H_k} \mu_k \geq 1 \\ 1 \mu_k < 1 \end{cases} \quad (37)$$

where $\text{trace}(\cdot)$ is the trace of the corresponding matrix, and C_k is the covariance of the residual sequence of outputs and can be expressed as

$$C_k = \begin{cases} \varepsilon_1 \varepsilon_1^T k=1 \\ \frac{\rho C_{k-1} + \varepsilon_k \varepsilon_k^T}{1+\rho} k \geq 2 \end{cases} \quad (38)$$

where ρ is the forgetting factor, and its range is set as 0.95~0.99; ε_k is the output residual sequence, and $\varepsilon_k = y_k - \hat{y}_{k|k-1}$.

3.2.2. The State Noise Tracking Coefficient

In Formula (32), the state covariance square-root matrix $S_{k|k-1}$ is directly affected by the Q_{k-1} . If the Q_{k-1} diverges, the $S_{k|k-1}$ will further diverge. In this paper, the variation of the matrix elements of the $S_{k|k-1}$ based on its historical data is used to reflect the variation trend of Q_{k-1} . The updated state covariance square-root matrix $S_{k|k-1}^c$ can be expressed as

$$\begin{cases} S_{k|k-1}^c = \lambda_k S_{k|k-1} \lambda_k^T + \delta_k \sqrt{Q_{k-1}} \delta_k^T \\ \delta_k = \text{diag}[m_k, m_k, m_k, \dots, m_k] \end{cases} \quad (39)$$

where $S_{k|k-1}^c$ is the corrected state covariance square-root matrix at time k , and δ_k is the state noise tracking coefficient, whose dimension is n columns. m_k is the matrix element of the state noise tracking coefficient. Its value is attained by comparing the element mean

value of the state covariance square-root matrix in the iteration process. The assignment process of m_k is described as follows:

- (1) Initialize the m_k and its dimension to n columns.
- (2) $P_{k|k-1}^{(i)}$ is set as an element in the i th row and i th column of the state covariance square-root matrix at time k . We set the mean of the elements in m adjacent square-root matrices as a parameter and definite A and B as the pairwise comparisons between adjacent parameters, which can be described as

$$A = \frac{1}{m} \sum_{k=m}^{k=2m-1} S_{k|k-1}^{(i)} - \frac{1}{m} \sum_{k=2m}^{k=3m-1} S_{k|k-1}^{(i)} \quad (40)$$

$$B = \frac{1}{m} \sum_{k=2m}^{k=3m-1} S_{k|k-1}^{(i)} - \frac{1}{m} \sum_{k=3m}^{k=4m-1} S_{k|k-1}^{(i)} \quad (41)$$

By comparing A and B, six outcomes will be attained:

$$\begin{cases} A < B < 0 \text{ (I)} \\ A < 0 < B \text{ (II)} \\ B < A < 0 \text{ (III)} \\ B < 0 < A \text{ (IV)} \\ 0 < A < B \text{ (V)} \\ 0 < B < A \text{ (VI)} \end{cases} \quad (42)$$

- (3) Attain the updated m_k . If the outcome does not match outcome (II) or outcome (V), the m_k should not be modified. If the calculated result matches outcome (II) or outcome (V), the m_k should be reassigned. If the value of Q_0 is higher than 2% of the U_{OC} , the Q_0 is judged to be too large, and the state noise tracking coefficient should be shrunk, and then the value $m_k = [1 - \gamma, 1 - \gamma, 1 - \gamma, \dots, 1 - \gamma]$ should be assigned. If the Q_0 value is less than 2% of the U_{OC} , the Q_0 is judged to be too small, and the state noise tracking coefficient should be amplified, and then the value $m_k = [1 + \gamma, 1 + \gamma, 1 + \gamma, \dots, 1 + \gamma]$ should be assigned, where γ is the correction coefficient.
- (4) According to m_k and Formula (39), we can get the state noise tracking coefficient δ_k .
- (5) The δ_k and λ_k are used as inputs to form the dual-coefficient tracker.
- (6) The dual-tracking coefficient λ_k and δ_k are put into the ISRUKF to calculate the updated state covariance square-root matrix $S_{k|k-1}^c$, which can be illustrated as

$$\begin{cases} r_k = qr\{[\lambda_k \sqrt{w_i^c}(x_{i=1:2n,k|k-1} - \hat{x}_{k|k-1}), \delta_k \sqrt{Q_{k-1}}]^T\} \\ S_{k|k-1}^c = r_k^T \end{cases} \quad (43)$$

Figure 3 shows the diagram of the dual-coefficient tracker.

3.3. Battery SOC Estimation Procedure Based on Dual-Coefficient Tracking ISRUKF

According to the above analysis, the flow diagram of the battery SOC estimation based on the developed method shown in Figure 4 can be expressed as follows:

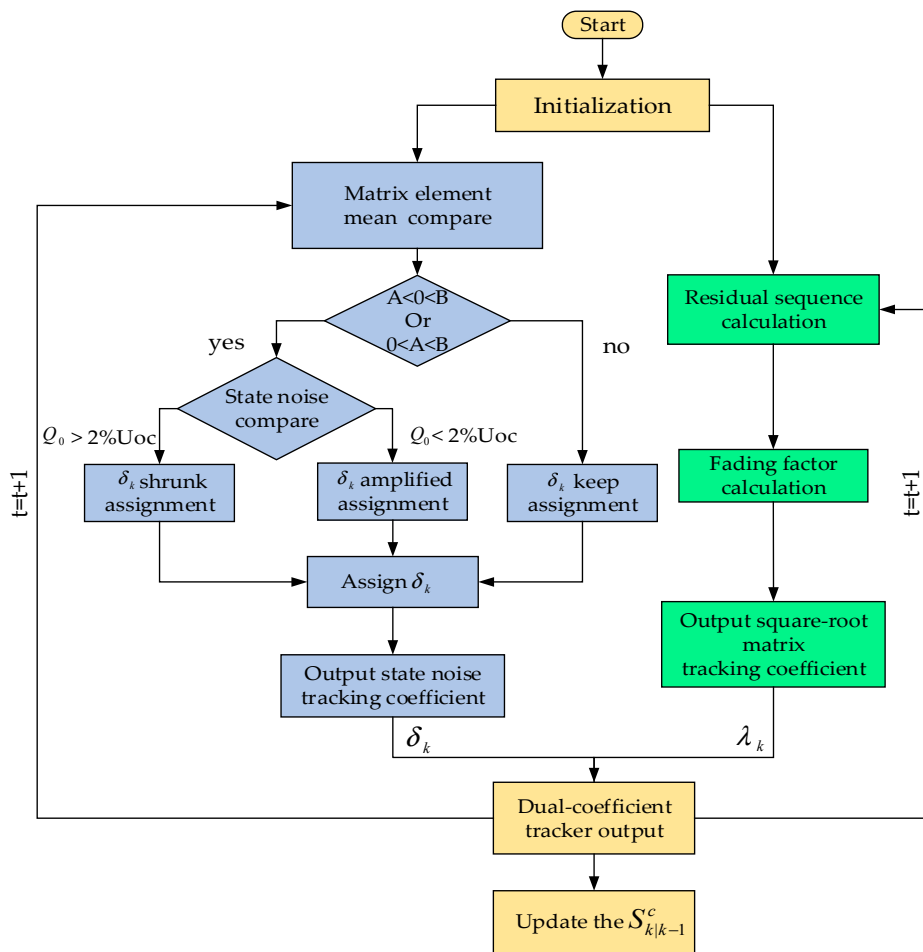


Figure 3. Diagram of dual-coefficient tracker.

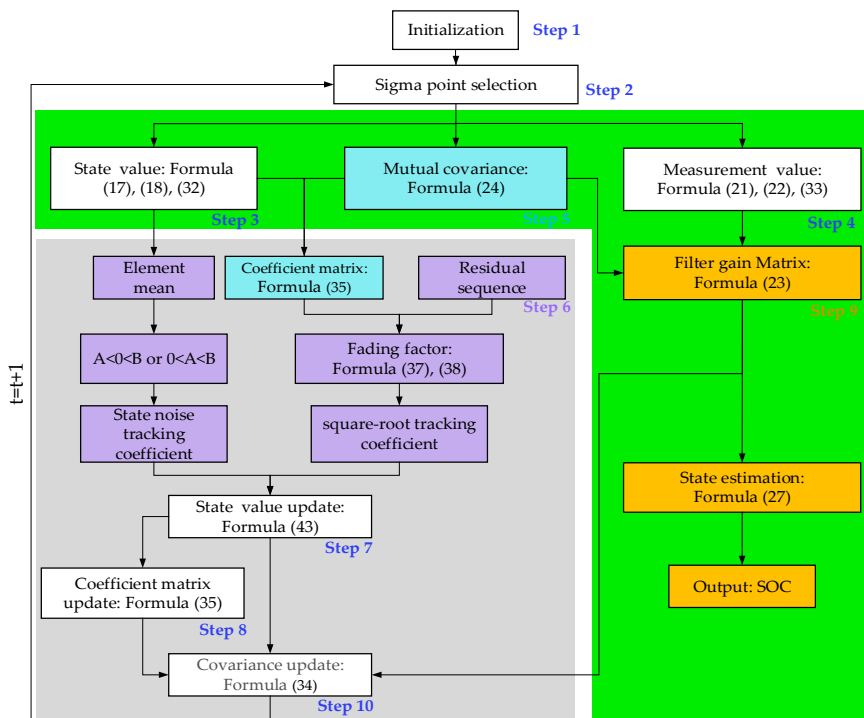


Figure 4. Flow diagram of the battery SOC estimation based on the developed method.

- Step 1: Initialize the mean (x_0) and the state covariance square root (S_0) by Formula (13), and initialize the λ_0 and δ_0 ;
- Step 2: Assign weights w^m and w^c and obtain sampling points $x_{i,k}$ by Formulas (14) and (16);
- Step 3: Time update for the state estimation $x_{i,k|k-1}$, $\hat{x}_{k|k-1}$, and $S_{k|k-1}$ by Formulas (17), (18) and (32);
- Step 4: Measurement update $y_{i,k|k-1}$, $\hat{y}_{k|k-1}$, and S_Z by Formulas (21), (22), and (33);
- Step 5: Calculate the mutual covariance P_{xy} by Formula (24) and estimate the coefficient matrix of measurement function H_k by Formula (35);
- Step 6: Calculate the λ_k by Formulas (36), (37) and (38); attain the mean values of the state covariance square-root matrix by Formulas (40) and (41) and compare A and B by Formula (42) to determine the assignment of δ_k ;
- Step 7: The λ_k and δ_k are substituted into Formula (43) to update the state covariance square-root matrix $S_{k|k-1}^c$;
- Step 8: Use $S_{k|k-1}^c$ to update the coefficient matrix of the measurement function by Formula (35);
- Step 9: Calculate the filtering gain matrix L_k by Formula (23) and the output estimation of the SOC by Formula (27);
- Step 10: Attain the state covariance square-root optimal estimation matrix $S_{k|k}$ by the updated state covariance square-root matrix and the update coefficient matrix of the measurement function via Formula (34) and start the next iteration process.

4. Simulation and Experimental Results and Analysis

4.1. Test Platform and Experiment Parameters

The test platform shown in Figure 5 consists of an Arbin-BT2000 battery test system, lithium-ion batteries, and a computer. The battery test system is used for the testing of the batteries to attain battery parameters, such as the battery current, voltage, charge capacity, discharge capacity, internal resistance, etc. The single-channel voltage measurement range of the battery test system is 0~5 V, and the resolution of the measured voltage is $\pm 0.01\%$ of the full scale. The computer can record and process experimental data including the battery voltage, current, internal resistance, etc. Lithium-ion batteries are connected to the battery test system and can be continuously charged and discharged.

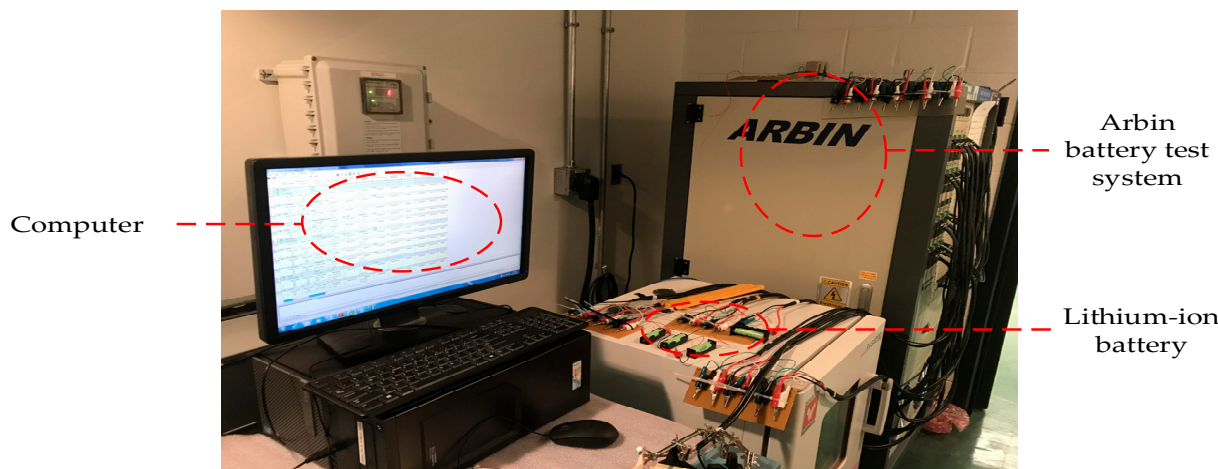


Figure 5. Schematic of the lithium-ion battery test platform.

To validate the SOC estimation accuracy using the developed ISRUKF, three test schedules were conducted via some comparisons of simulation results with experimental data in the discharging process. In each test, the battery simulation and experiment were carried out at the temperature of 25 °C. The batteries were discharged with the initial SOC

of 0.9 and were ended when the SOC was 0.2. The simulation and experimental parameters of batteries are listed in Table 1.

Table 1. The coefficients of battery performance parameters.

Normal Voltage Upper Cut-Off Voltage	3.7 V 4.2 V	Battery Capacity Lower Cut-Off Voltage	860 mAh 3.2 V
a_0	−0.915	a_1	40.867
a_3	0.537	a_4	0.499
b_0	0.1463	b_1	30.27
b_3	0.0584	b_4	0.1747
c_0	0.1063	c_1	62.49
d_0	−200	d_1	138
e_0	0.0712	e_1	61.4
f_0	−3083	f_1	180
			5088

4.2. Comparison of SOC Estimation Accuracy Using the Developed ISRUKF, SRUKF, and UKF with Different Covariance Q_k

In this section, the comparison of SOC estimation accuracy between the developed ISRUKF, SRUKF, and UKF is carried out when the Q_k is 0.005 and 0.01, respectively, to verify the accuracy of the developed ISRUKF. Figure 6 shows the comparative results of the SOC and battery voltage using the three algorithms when the Q_k is set as 0.005.

Figure 6a,b show the SOC experiment and estimation results and the corresponding absolute errors by the different methods. The UKF, SRUKF, and developed ISRUKF can be used to estimate the SOC with different estimation accuracy. Compared to the UKF and the SRUKF, the developed ISRUKF shows the highest SOC estimation accuracy in the discharging process.

As shown in Figure 6b, the SOC estimation errors using the developed ISRUKF are constantly kept below 0.01 given its dual-coefficient tracker, which can reduce state noise accumulative calculation errors. The SOC estimation errors using the UKF and SRUKF gradually increase from 0.01 to 0.06, even to divergence. Figure 6c,d show the battery voltage experiment and estimation results and the corresponding absolute errors by the different methods. Similar to the SOC estimation results, the estimated battery voltage using the UKF, SRUKF, and developed ISRUKF can effectively capture the experiment results. However, the estimated battery voltage based on the developed ISRUKF shows the lowest voltage errors within 0.01 V, as shown in Figure 6d. Moreover, under the same conditions of achieving 270,000 sampling points in the calculation step of 0.01 s, the calculation time of the SOC using the UKF, the SRUKF, and the developed method is 7.5 s, 7.6 s, and 7.7 s, respectively. Compared to the UKF and the SRUKF, the developed method spends almost an equal amount of time to estimate the SOC, but it can achieve the highest SOC estimation accuracy within 1.5% error, and the SOC errors of the UKF and the SRUKF are 6.7% and 5.5%, respectively, as shown in Figures 6b and 7b.

Figure 7 illustrates the SOC estimation results using the UKF, SRUKF, and developed ISRUKF when the Q_k is set as 0.01. Figure 7a,b present the SOC experiment and estimation results and the corresponding absolute errors by the different methods. Figure 7c,d show the battery voltage estimation results and the corresponding absolute errors using the three methods.

The estimation accuracy of the SOC and battery voltage using the developed ISRUKF is the highest compared to the UKF and the SRUKF. For example, the SOC errors are constantly controlled below 0.01, as shown in Figure 7b, and the batteries' voltage errors are kept within 0.015 V, which is about 0.5% of the batteries' nominal voltage, as shown in Figure 7d.

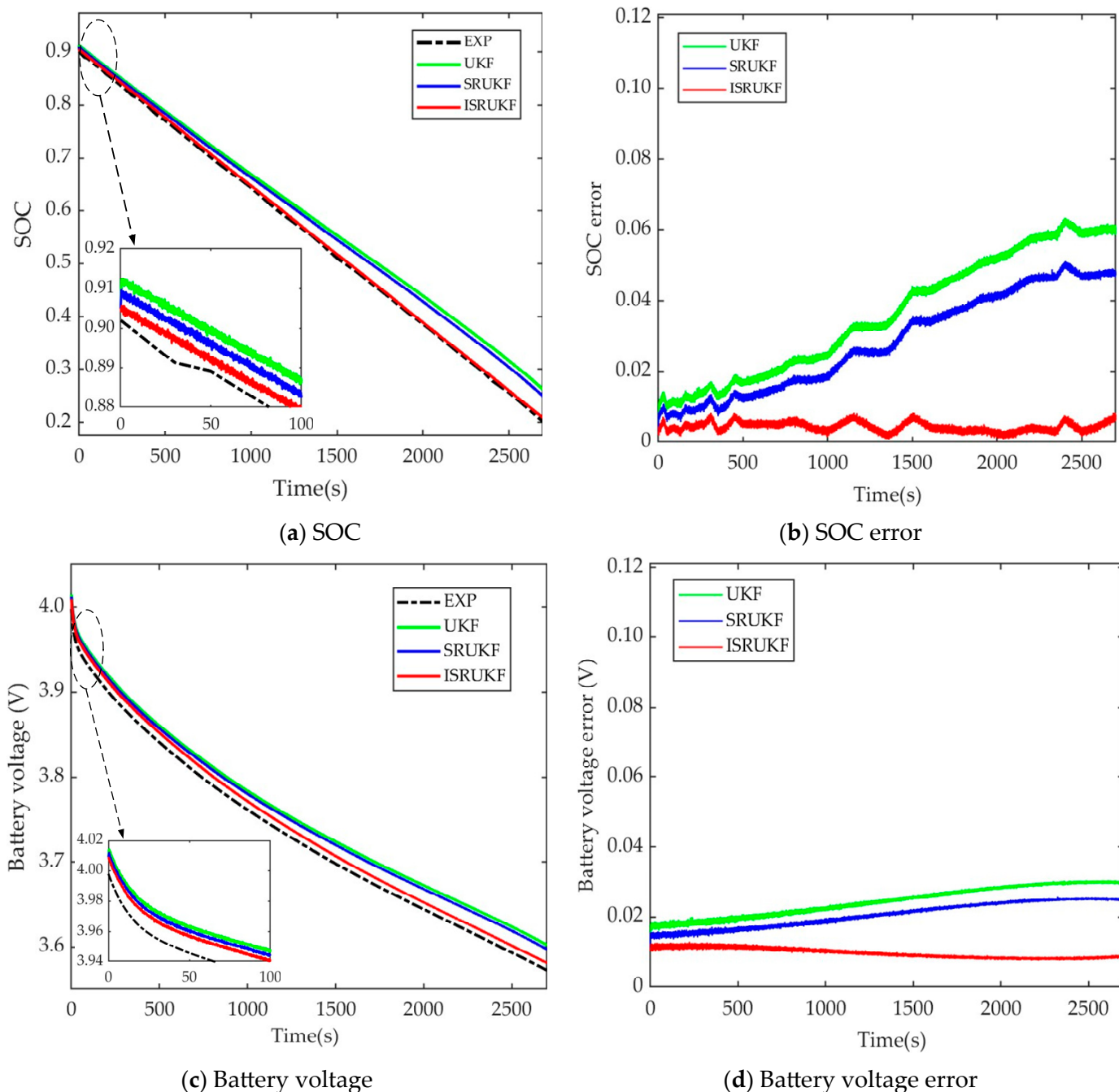


Figure 6. SOC estimation results using three different algorithms when the Q_k is set as 0.005.

Moreover, with the help of the QR decomposition method (which can overcome the problem of the pseudo-positive definiteness of the covariance matrix), the errors of the estimated SOC and battery voltage estimation using the developed ISRUKF are stable or not divergent. However, the errors of the estimated SOC and battery voltage estimation using the UKF and the SRUKF gradually increase and even diverge in the discharging process shown in Figure 6b,d and Figure 7b,d. It is further proven that the developed ISRUKF based on a dual-coefficient tracker can accurately estimate the SOC for lithium-ion batteries and effectively avoid SOC divergence.

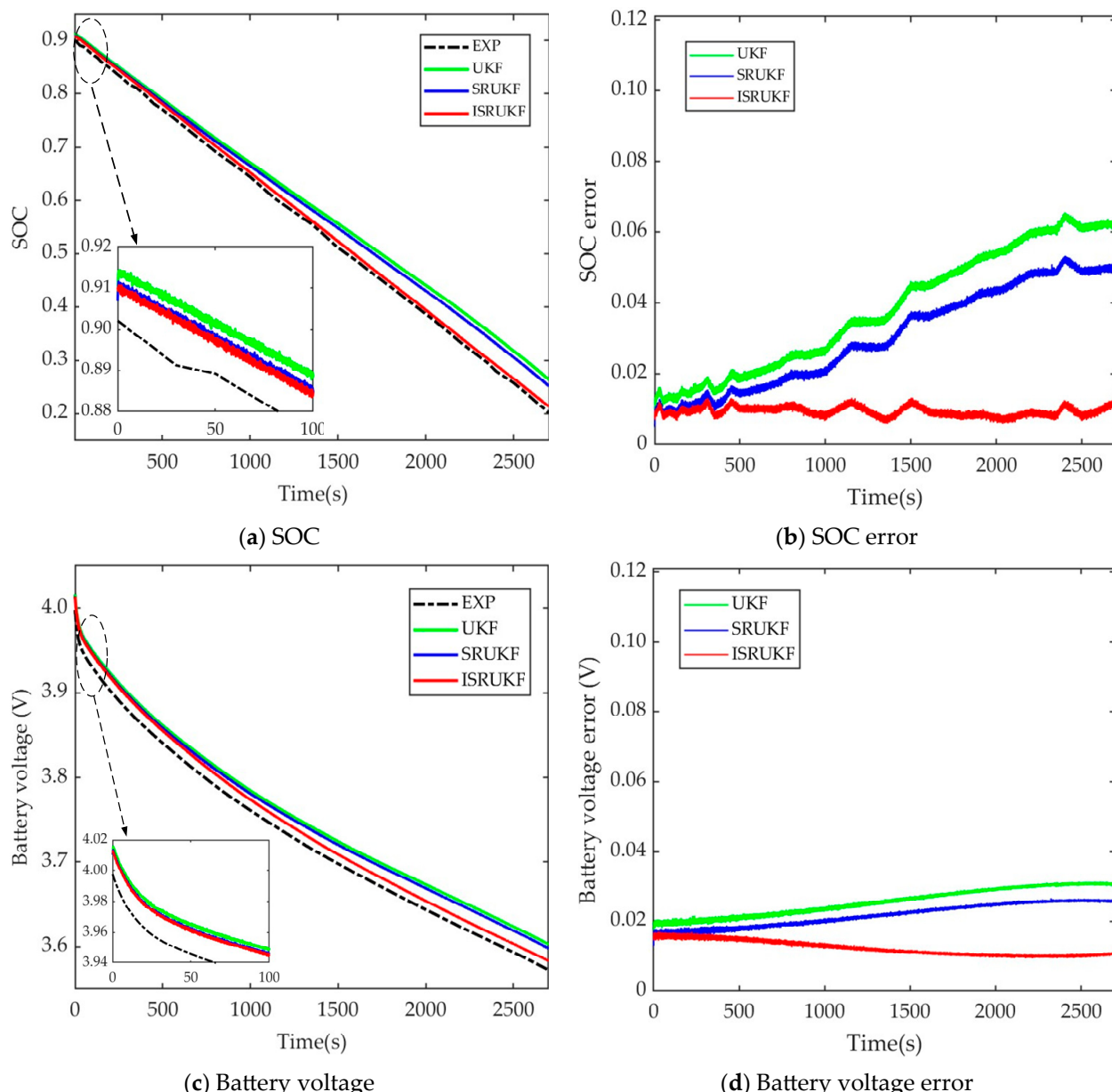


Figure 7. SOC estimation results using three different algorithms when the Q_k is set as 0.01.

4.3. Comparison of SOC Estimation Results Using Different ISRUKFs, the ISRUKF with Standard STF and the Developed ISRUKF

In this section, a comparison of SOC estimation accuracy using different ISRUKFs (including the developed ISRUKF and the ISRUKF with the standard STF) is carried out to further validate the effectiveness of the developed ISRUKF. Figure 8 shows the SOC estimation accuracy using different ISRUKFs when the Q_k is set as 0.005. Figure 8a compares the estimated SOC using the developed ISRUKF (in red) versus the ISRUKF with the standard STF (in green). It is shown that the SOC based on the ISRUKF with the standard STF can consistently follow the experimental results at the beginning of the discharging process, but this SOC deviates further and further from the experiment results as the discharging process moves forward. Figure 8b shows the corresponding SOC absolute error using the different ISRUKFs. Due to the dual-coefficient tracker reducing state noise accumulative calculation errors, the SOC absolute error using the developed ISRUKF (in red) is always lower than the SOC absolute error using the ISRUKF with the standard STF.

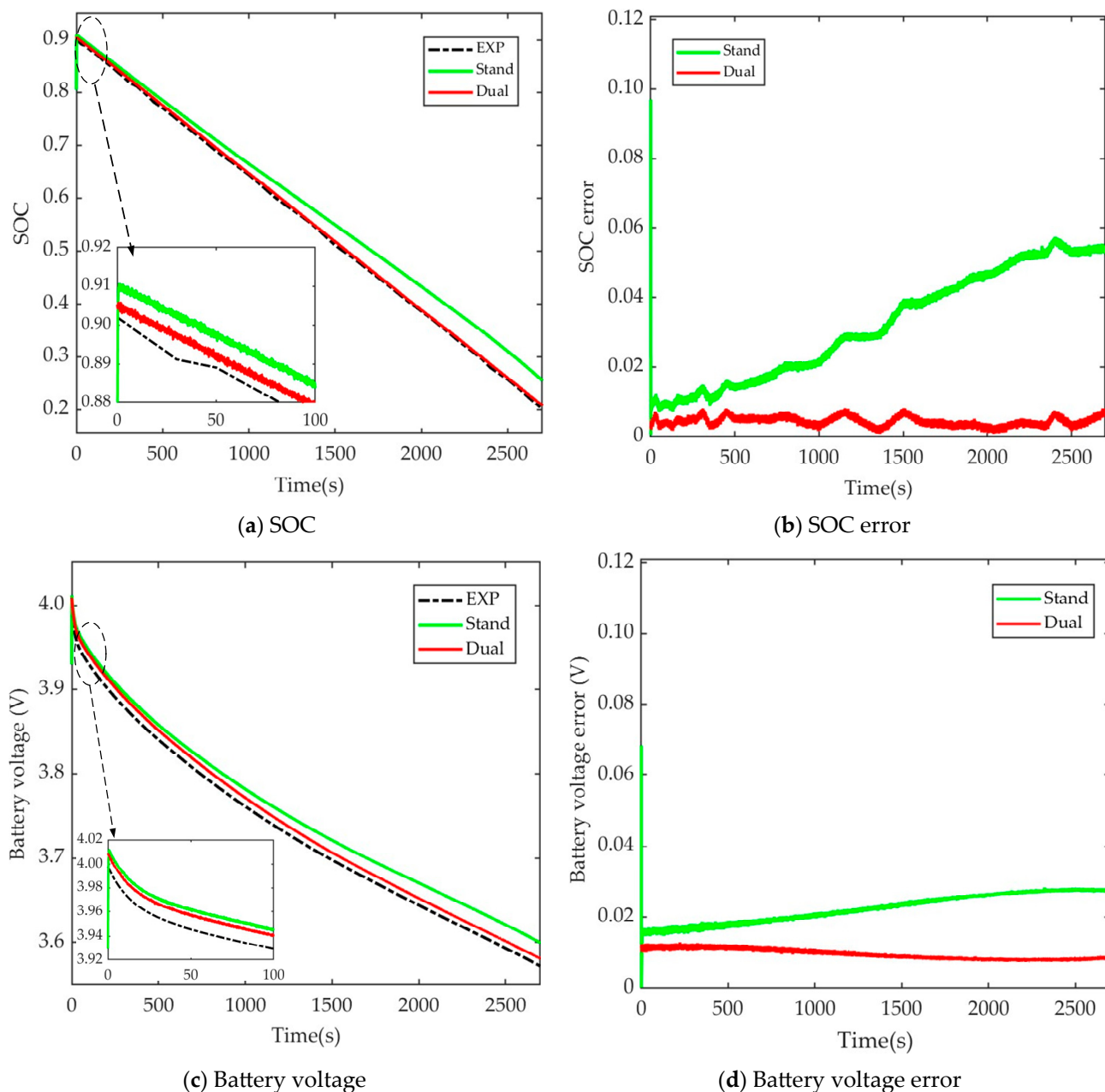


Figure 8. SOC estimation accuracy using different ISRUUKFs when the Q_k is set as 0.005.

Without the ability of adjusting the state noise tracking coefficient δ_k , the ISRUUKF with the standard STF cannot reduce the state noise error accumulation in the iteration process of the UKF, which leads to the SOC absolute error based on this ISRUUKF increasing continuously. For example, the SOC absolute error using the developed ISRUUKF is constantly kept within 0.01, but the SOC absolute error using the ISRUUKF with the standard STF gradually increases from 0.01 to 0.05. Figure 8c,d describe the battery voltage estimation results and the corresponding absolute errors using the different ISRUUKFs. It is found that the battery voltage profile based on the developed method can track the experimental results accurately in the whole discharging process with a lower absolute error compared to using the ISRUUKF with the standard STF. Therefore, compared to the ISRUUKF with the standard STF, the developed method can achieve higher SOC and voltage estimation accuracy.

4.4. SOC Estimation by the Developed ISRUKF with Different Covariance Q_k

To verify the effectiveness and adaptation of the developed ISRUKF, a comparison of SOC estimation accuracy is performed when the Q_k is different. The Q_k is randomly set to 0.001, 0.005, and 0.01, respectively. Figure 9 shows SOC estimation results using the developed ISRUKF with different Q_k . Figure 9a,b illustrate the SOC estimation accuracy and its corresponding absolute error by the developed method with various noise statistics. It is noted that the estimated SOC using the developed method can exactly capture the experimental results, and the corresponding SOC absolute errors are stable and small despite the various noise statistics. As shown in Figure 9b, when the noise statistics are set to 0.001, 0.005, and 0.01, respectively, the highest SOC absolute error is controlled below 0.015, and the lowest SOC absolute error is controlled below 0.005 (means 0.5%).

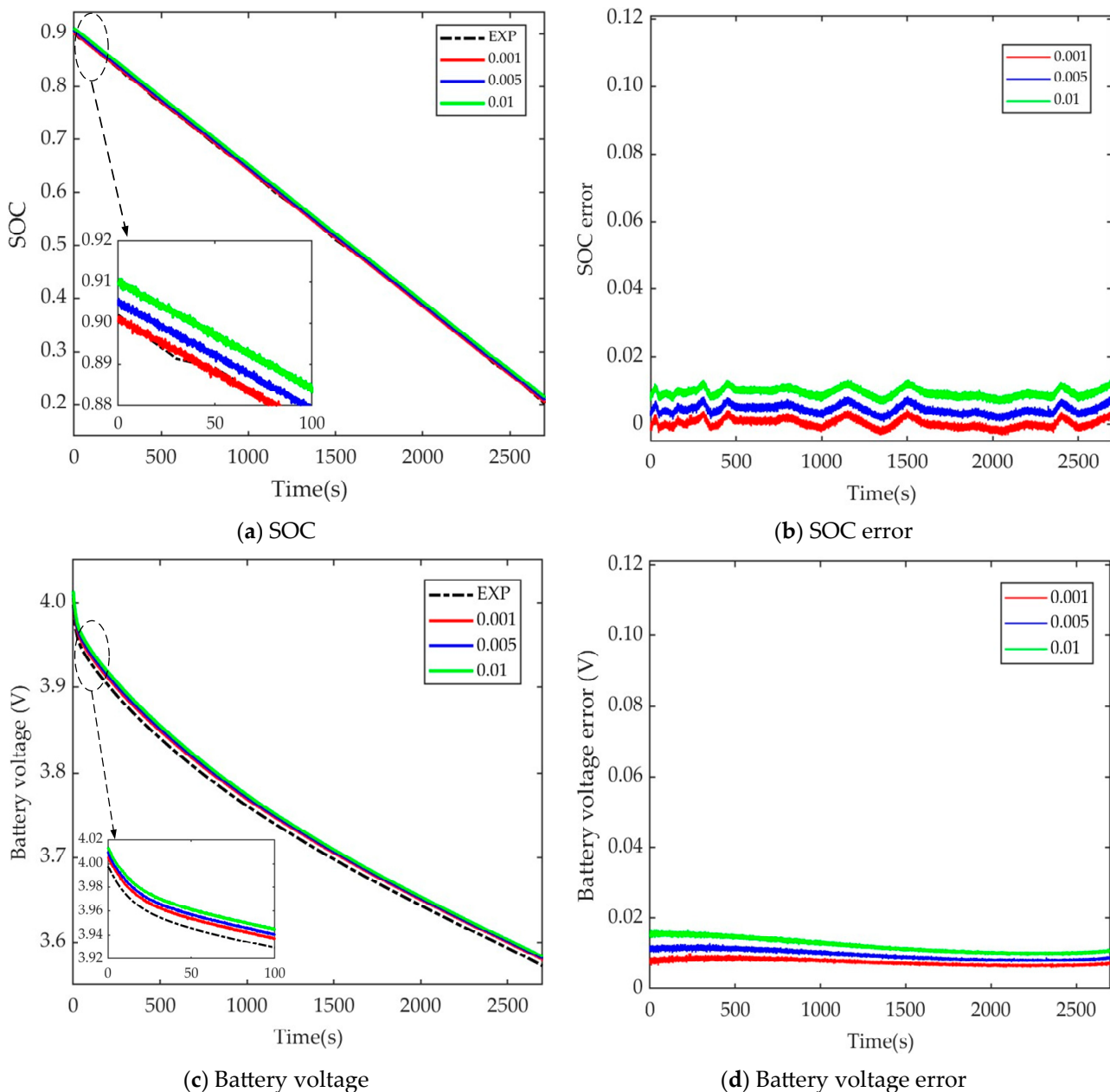


Figure 9. SOC estimation by the developed ISRUKF with different Q_k .

Figure 9c,d show the battery voltage estimation and the corresponding absolute error using the developed ISRUKF with different noise statistics. With the help of the dual-coefficient tracker, the developed method can reduce state noise accumulative calculation

errors; in turn, this contributes to gradually reducing the battery voltage deviation from the experimental results and improving its estimation accuracy. Therefore, the developed ISRUKF can not only precisely estimate the SOC of lithium-ion batteries but also shows good robustness when Q_k varies.

4.5. Discussions

As a nonlinear system of the battery system, it is difficult to estimate the SOC accurately due to the influence of batteries' incorrect noise statistics, such as the battery model error and the round-off error of the filter. To verify the SOC estimation precision using the developed method based on the ISRUKF with a dual-coefficient tracker, three test schedules are carried out. With the help of the dual-coefficient tracker, which can track and correct the batteries' model noise error accumulation, the SOC estimation errors using the developed ISRUKF show the highest precision (below 1.5%) compared with the UKF (6.7%) and the SRUKF (5.5%) when the Q_k is 0.005 and 0.01, respectively. Moreover, because the ISRUKF based on the QR decomposition method can overcome the problem of the pseudo-positive definiteness of the batteries' model covariance, the estimated SOC errors and battery voltage errors using the developed method are kept within a stable range. However, the estimated SOC errors based on the UKF and the SRUKF gradually increase and even diverge.

However, due to not considering the residual sequence of the measurement noise in the dual-coefficient tracker, the SOC estimation accuracy using the developed method based on the dual-coefficient tracker is degraded. In addition, because of the addition of the tracking coefficient calculation, it takes more time for the developed method to accurately estimate the SOC of batteries compared to the UKF and the SRUKF. Some measures should be taken to optimize the iteration process to reduce the calculation time of the developed method.

5. Conclusions

Precise SOC estimation can contribute to protecting and extending the life of lithium-ion batteries. However, the SOC estimation accuracy estimated by the UKF and SRUKF is degraded when the noise statistics arise. Therefore, an SOC estimation method based on a dual-coefficient tracking improved square-root unscented Kalman filter (ISRUKF) was developed in this paper for lithium-ion batteries. Compared to the SRUKF and the UKF, the developed ISRUKF shows the highest SOC estimation accuracy with an SOC error below 1.5% when the Q_k is 0.005 and 0.01, but the SOC error using the UKF and the SRUKF is 6.7% and 5.5%, respectively. At the same time, with the help of its dual-coefficient tracker, which can reduce state noise accumulative calculation errors, the SOC absolute error using the developed ISRUKF is always lower than the SOC absolute error using the ISRUKF with the standard STF when the Q_k is constant (set as 0.005). For example, the SOC error using the ISRUKF with the standard STF gradually increases from 0.01 to 0.05, and its maximum error is about 5%, while the developed ISRUKF can keep the SOC error under 1.1%. Moreover, the developed ISRUKF can not only precisely estimate the SOC of lithium-ion batteries with the lowest SOC absolute error of 0.5% but also shows good robustness when the state noise statistics are set to 0.001, 0.005, and 0.01, respectively.

Future work includes the investigation of optimizing the dual-coefficient tracker. The SOC estimation accuracy of lithium-ion batteries is reduced using the developed method because of ignoring the measurement noise and corresponding noise covariance of the batteries, such as the measurement errors of the terminal voltage and current of the batteries. The optimization of the batteries' measurement noise in the developed method will be performed in future works. Additionally, further research will also be carried out to explore reducing the calculation time of the developed ISRUKF. It is important for online SOC estimation to reduce the calculation time of the ISRUKF and other algorithms.

Author Contributions: Methodology and writing, S.P.; Original draft preparation and data curation, A.Z.; Project administration and data curation, D.L.; Validation and data curation, M.C.; Software and methodology, J.K.; Content organization and delivery, M.P. All authors have read and agreed to the published version of the manuscript.

Funding: This research was funded by the Jiangsu University “Qinglan Project” (2021-11) grant number: xjr2021052.

Acknowledgments: We are grateful to the Jiangsu University “Qinglan Project” (2021-11) and school-level research projects of the Yancheng Institute of Technology (xjr2021052) for supporting this research. The authors also thank the more than 150 companies and organizations that support research activities at the Center for Advanced Life Cycle Engineering (CALCE) at the University of Maryland and the Centre for Advanced Innovations in Reliability and Safety (CAIRS).

Conflicts of Interest: The authors declare no conflict of interest. The funders had no role in the design of the study; in the collection, analyses, or interpretation of data; in the writing of the manuscript; or in the decision to publish the results.

Nomenclature

SOC	state of charge (-)
KF	Kalman filter (-)
EKF	extended Kalman filter (-)
UKF	unscented Kalman filter (-)
SRUKF	square-root unscented Kalman filter (-)
AUKF	adaptive unscented Kalman filter (-)
STF	strong tracking filter (-)
OCV	open-circuit voltage (V)
ECM	equivalent circuit model (-)
U_{OC}	open-circuit voltage of the batteries (V)
R_0	internal resistance of the batteries (Ω)
R_L	concentration resistance of the batteries (Ω)
C_L	concentration capacitance of the batteries (F)
R_S	electrochemical resistance (Ω)
C_S	electrochemical capacitance (F)
I_t	current of the batteries (A)
U_t	terminal voltage of the batteries (V)
$a_0 \sim a_5$	coefficient of the equation (-)
$b_0 \sim b_5$	coefficient of the equation (-)
$c_0 \sim c_5$	coefficient of the equation (-)
$d_0 \sim d_5$	coefficient of the equation (-)
$e_0 \sim e_5$	coefficient of the equation (-)
$f_0 \sim f_5$	coefficient of the equation (-)
SOC_0	initial value of SOC (-)
η	coulomb efficiency (-)
Q_N	nominal capacity of the batteries (Wh)
U_S	electrochemical voltage of the batteries (V)
U_L	concentration voltage of the batteries (V)
Δt	sampling time (s)
τ_1	time parameter (s)
τ_2	time parameter (s)
w_k	state noise (-)
v_k	measurement noise (-)
x_k	system state vector (-)
y_k	system measurement vector (-)
u_k	system input vector (V)

$f(\cdot)$	nonlinear state model (-)
$g(\cdot)$	nonlinear measurement model (-)
r	mean of the measurement noise (-)
q	mean of the state noise (-)
R	covariance value of measurement noise (-)
Q	covariance value of state noise (-)
x_0	initial mean (-)
S_0	initial state covariance square root (-)
$E(\cdot)$	expectation mean value (-)
$(\cdot)^T$	matrix transpose operation (-)
n	dimension of the state vector (-)
α	scaling parameter (-)
h	column factor (-)
w^m	variance weight factor (-)
w^c	mean weight factor (-)
β	error magnitude of the higher-order term (-)
$S_{k k-1}^*$	updated state calculation value (-)
$qr(\cdot)$	QR decomposition (-)
$S_{k k-1}$	state covariance square-root matrix (-)
$cholupdate(\cdot)$	Cholesky decomposition (-)
P_{xy}	mutual covariance (-)
S_z^*	updated calculation measurement
S_z	measurement covariance square-root matrix (-)
$S_{k k}$	state covariance square-root optimal estimation matrix (-)
$P_{k k-1}$	state covariance matrix (-)
q_k	upper triangular matrix (-)
r_k	orthogonal matrix (-)
e	identity matrix of order n (-)
H_k	coefficient matrix of the measurement function (-)
λ_k	fading factor (-)
$trace(\cdot)$	trace of the corresponding matrix (-)
C_k	covariance of the residual sequence of outputs (-)
ρ	forgetting factor (-)
ε_k	output residual sequence
$S_{k k-1}^c$	corrected state covariance square-root matrix (-)
δ_k	state noise tracking coefficient (-)

References

- Renxin, X.; Yanwen, H.; Wei, Z.; Zhaojun, C. A novel approach to estimate the state of charge for lithium-ion battery under different temperatures incorporating open circuit voltage online identification. *J. Energy Storage* **2023**, *67*, 107509. [[CrossRef](#)]
- Meng, J.; Yue, M.; Diallo, D. Nonlinear extension of battery constrained predictive charging control with transmission of Jacobian matrix. *Int. J. Electr. Power Energy Syst.* **2023**, *146*, 108762. [[CrossRef](#)]
- Qiao, J.; Wang, S.; Yu, C.; Yang, X.; Fernandez, C. A chaotic firefly-Particle filtering method of dynamic migration modeling for the state-of-charge and state-of-health co-estimation of a lithium-ion battery performance. *Energy* **2023**, *263*, 126164. [[CrossRef](#)]
- Yu, Q.; Liu, Y.; Long, S.; Jin, X.; Li, J.; Shen, W. A Branch Current Estimation and Correction Method for a Parallel Connected Battery System Based on Dual BP Neural Networks. *Green Energy Intell. Transp.* **2022**, *1*, 100029. [[CrossRef](#)]
- Peng, S.; Zhu, L.; Dou, Z.; Liu, D.; Yang, R.; Pecht, M. Method of Site Selection and Capacity Setting for Battery Energy Storage System in Distribution Networks with Renewable Energy Sources. *Energies* **2023**, *16*, 3899. [[CrossRef](#)]
- Chen, C.; Xiong, R.; Yang, R.; Li, H. A novel data-driven method for mining battery open-circuit voltage characterization. *J. Green Energy Intell. Transp.* **2022**, *1*, 100001. [[CrossRef](#)]
- Chen, B.; Jiang, H.; Chen, X.; Li, H. Robust state-of-charge estimation for lithium-ion batteries based on an improved gas-liquid dynamics model. *Energy* **2022**, *238*, 122008. [[CrossRef](#)]
- Xia, L.; Wang, S.; Yu, C.; Fan, Y.; Li, B.; Xie, Y. Joint estimation of the state-of-energy and state-of-charge of lithium-ion batteries under a wide temperature range based on the fusion modeling and online parameter prediction. *J. Energy Storage* **2022**, *52*, 105010. [[CrossRef](#)]
- Wassiliadis, N.; Kriegler, J.; Gamra, K.A.; Lienkamp, M. Model-based health-aware fast charging to mitigate the risk of lithium plating and prolong the cycle life of lithium-ion batteries in electric vehicles. *J. Power Sources* **2023**, *561*, 232586. [[CrossRef](#)]

10. Liu, Z.; Zhao, Z.; Qiu, Y.; Jing, B.; Yang, C. State of charge estimation for Li-ion batteries based on iterative Kalman filter with adaptive maximum correntropy criterion. *J. Power Sources* **2023**, *580*, 233282. [[CrossRef](#)]
11. Zhao, X.; Jung, S.; Wang, B.; Xuan, D. State of charge estimation of lithium-ion battery based on improved adaptive boosting algorithm. *J. Energy Storage* **2023**, *71*, 108047. [[CrossRef](#)]
12. Li, X.; Wang, Z.; Zhang, L. Co-estimation of capacity and state-of-charge for lithium-ion batteries in electric vehicles. *Energy* **2019**, *174*, 33–44. [[CrossRef](#)]
13. Yu, Q.; Huang, Y.; Tang, A.; Wang, C.; Shen, W. OCV-SOC-Temperature Relationship Construction and State of Charge Estimation for a Series-Parallel Lithium-Ion Battery Pack. *IEEE Trans. Intell. Transp. Syst.* **2023**, *24*, 6362–6371. [[CrossRef](#)]
14. Wang, C.; Zhang, X.; Yun, X.; Fan, X. A novel hybrid machine learning coulomb counting technique for state of charge estimation of lithium-ion batteries. *J. Energy Storage* **2023**, *63*, 107081. [[CrossRef](#)]
15. Li, K.; Gao, X.; Liu, C.; Chang, C.; Li, X. A novel Co-estimation framework of state-of-charge, state-of-power and capacity for lithium-ion batteries using multi-parameters fusion method. *Energy* **2023**, *269*, 126820. [[CrossRef](#)]
16. Zhu, R.; Duan, B.; Zhang, J.; Zhang, Q.; Zhang, C. Co-estimation of model parameters and state-of-charge for lithium-ion batteries with recursive restricted total least squares and unscented Kalman filter. *Appl. Energy* **2020**, *277*, 115494. [[CrossRef](#)]
17. Xia, B.; Cui, D.; Sun, Z.; Lao, Z.; Zhang, R.; Wang, W.; Sun, W.; Lai, Y.; Wang, M. State of charge estimation of lithium-ion batteries using optimized Levenberg-Marquardt wavelet neural network. *Energy* **2018**, *153*, 694–705. [[CrossRef](#)]
18. Song, Q.; Wang, S.; Xu, W.; Shao, Y.; Fernandez, C. A novel joint support vector machine-cubature Kalman filtering method for adaptive state of charge prediction of lithium-ion batteries. *Int. J. Electrochem. Sci.* **2021**, *16*, 210823. [[CrossRef](#)]
19. Tagade, P.; Hariharan, K.S.; Gambhire, P.; Kolake, S.M.; Song, T.; Oh, D.; Yeo, T.; Doo, S. Recursive Bayesian filtering framework for lithium-ion cell state estimation. *J. Power Sources* **2016**, *306*, 274–288. [[CrossRef](#)]
20. Zhu, W.; Guo, B.; Li, Y.; Yang, Y.; Xie, C.; Jin, J.; Gooi, H.B. Uncertainty quantification of proton-exchange-membrane fuel cells degradation prediction based on Bayesian-Gated Recurrent Unit. *eTransportation* **2023**, *16*, 100230. [[CrossRef](#)]
21. Jiang, B.; Dai, H.; Wei, X.; Xu, T. Joint estimation of lithium-ion battery state of charge and capacity within an adaptive variable multi-timescale framework considering current measurement offset. *Appl. Energy* **2019**, *253*, 113619. [[CrossRef](#)]
22. Plett, G.L. Extended Kalman filtering for batteries management systems of LiPB-based HEV batteries packs: Part 2. Modeling and identification. *J. Power Sources* **2004**, *134*, 262–276. [[CrossRef](#)]
23. Chai, H.; Gao, Z.; Jiao, Z.; Yang, C. State of charge estimation for lithium-ion batteries based on an adaptive fractional-order cubature Kalman filter with initial value compensation. *J. Energy Storage* **2023**, *68*, 107544. [[CrossRef](#)]
24. Yang, F.; Xing, Y.; Wang, D.; Tsui, K.L. A comparative study of three model-based algorithms for estimating state-of-charge of lithium-ion batteries under a new combined dynamic loading profile. *Appl. Energy* **2016**, *164*, 387–399. [[CrossRef](#)]
25. Liu, S.; Deng, D.; Wang, S.; Luo, W.; Takyi-Aninakwa, P.; Qiao, J.; Li, S.; Jin, S.; Hu, C. Dynamic adaptive square-root unscented Kalman filter and rectangular window recursive least square method for the accurate state of charge estimation of lithium-ion batteries. *J. Energy Storage* **2023**, *67*, 107603. [[CrossRef](#)]
26. Aung, H.; Low, K.S. Temperature dependent state-of-charge estimation of lithium ion battery using dual spherical unscented Kalman filter. *IET Power Electron.* **2015**, *8*, 2026–2033. [[CrossRef](#)]
27. Menegaz, H.M.T.; Ishihara, J.Y. Unscented and square-root unscented Kalman filters for quaternionic systems. *Int. J. Robust Nonlinear Control* **2018**, *28*, 4500–4527. [[CrossRef](#)]
28. Wei, W.; Gao, S.; Zhong, Y.; Gu, C.; Hu, G. Adaptive square-root unscented particle filtering algorithm for dynamic navigation. *Sensors* **2018**, *18*, 2337. [[CrossRef](#)]
29. Asl, R.M.; Hagh, Y.S.; Simani, S.; Handroos, H. Adaptive square-root unscented Kalman filter: An experimental study of hydraulic actuator state estimation. *Mech. Syst. Signal Process.* **2019**, *132*, 670–691.
30. Zhu, Q.; Xu, M.; Liu, W.; Zheng, M. A state of charge estimation method for lithium-ion batteries based on fractional order adaptive extended kalman filter. *Energy* **2019**, *187*, 115880. [[CrossRef](#)]
31. Duan, L.; Zhang, X.; Jiang, Z.; Gong, Q.; Wang, Y.; Ao, X. State of charge estimation of lithium-ion batteries based on second-order adaptive extended Kalman filter with correspondence analysis. *Energy* **2023**, *280*, 128159. [[CrossRef](#)]
32. Peng, S.; Chen, C.; Shi, H.; Yao, Z. State of charge estimation of battery energy storage systems based on adaptive unscented Kalman filter with a noise statistics estimator. *IEEE Access* **2017**, *5*, 13202–13212. [[CrossRef](#)]
33. Xu, X.; Tang, S.; Ren, H.; Han, X.; Wu, Y.; Lu, L.; Feng, X.; Yu, C.; Xie, J.; Ouyang, M.; et al. Joint state estimation of lithium-ion batteries combining improved equivalent circuit model with electrochemical mechanism and diffusion process. *J. Energy Storage* **2022**, *56*, 106135. [[CrossRef](#)]

Disclaimer/Publisher’s Note: The statements, opinions and data contained in all publications are solely those of the individual author(s) and contributor(s) and not of MDPI and/or the editor(s). MDPI and/or the editor(s) disclaim responsibility for any injury to people or property resulting from any ideas, methods, instructions or products referred to in the content.